Title

Pressure dependence of the interfacial structure of potassium chloride films on iron

Journal

Thin Solid Films, 593

ISSN

0040-6090

Authors

Olson, Dustin

Gao, Hongyu

Tang, Chun

et al.

Publication Date

2015-10-01

DOI

10.1016/j.tsf.2015.09.065

Olsen D, Gao H, Tang C, Tysoe WT and Martini A (2015) "Pressure dependence of the interfacial structure of potassium chloride films on iron", Thin Solid Films, 593, 150.

DOI: 10.1016/j.tsf.2015.09.065

Pressure Dependence of the Interfacial Structure of Potassium Chloride Films on Iron

Dustin Olson[1], Hongyu Gao[2], Chun Tang[2], Wilfred T. Tysoe[1] and Ashlie Martini[2]

[1] Department of Chemistry and Laboratory for Surface Studies, University of Wisconsin-Milwaukee, Milwaukee, WI 53211, USA

[2]School of Engineering, University of California Merced, Merced CA 95343, USA

Abstract

Potassium chloride films on a clean iron surface are used as a model system to explore the interfacial structure of the films and the dependence of that structure on film thickness and pressure. The interfacial structure of one-, two-, three- and four-layer films is measured experimentally using low-energy electron diffraction. Those finding are then complemented by molecular dynamics simulations in which the atomic interaction between the film and substrate is tuned to match film thickness-dependent sublimation activation energy obtained from temperature-programmed desorption measurements. The resultant simulation reliably predicts the structure of thicker films and is then used to study the effect of pressure on the distribution of the lattice constant within and between each layer of the potassium chloride films. Findings indicate that both film thickness and pressure affect the structure within the films as well as the degree of registry between the film and adjacent substrate.

Keywords: Boundary lubrication, potassium chloride, molecular dynamics simulations, pressure dependence.

1. Introduction

The registry between a film and substrate has a profound influence on interfacial shear. A film that is in registry with the substrate will result in the largest friction force since all the atoms at the interface will simultaneously surmount the sliding potentials. Conversely, a lack of

commensurability between the atoms in the contacting interface would lead to a lower shear strength which does not scale linearly with contact area [1-5]. For thin films, commensurability may be dependent on the thickness of the film and, in the case of confined films, pressure. Therefore, understanding the friction properties of an interface requires first understanding the dependence of film structure on thickness and pressure.

This complex relationship has been explored using a simple alkali halide as a model boundary lubricating film. While alkali halides are not used as commercial boundary films, their structural simplicity and the availability of a wide range of alkali halides with varying lattice constant, along with their chemical inertness make them attractive candidates for fundamental study [6]. In particular, the shear strength S of KCl films has been measured experimentally in ultrahigh vacuum (UHV) where it is found that S varies linearly with contact pressure P; $S(P)=S_0+\alpha P$ where S_0 and α are constants [7]. Such linear variations in interfacial shear strength as a function of contact pressure are relatively common in tribological systems [8-10]. The specific system explored both in the previous and current study is KCl on Fe(100), which is particularly well suited for such studies since precise interaction potentials for computational models are already available for alkali halide films and it is relatively straightforward to prepare well-defined films in ultrahigh vacuum by KCl evaporation.

This model system has previously been investigated using density-functional theory (DFT) calculations of KCl films on an Fe(100) substrate [11]. However, the requirements of using periodic boundary conditions for the calculations necessitated using KCl films that were in registry with the iron substrate. Since the lattice mismatch between KCl and the 100 face of iron is significant (~7%), the resulting KCl film is strained. Nevertheless, these calculations revealed a relatively low barrier to sliding the KCl film against the Fe(100) face of ~ 0.7 kJ/mol that yielded a calculated shear strength that was in good agreement with experiment. In this case, it was proposed that the pressure-dependent shear strength arose because of the vertical motion of the atoms in the contact as they slid from one stable site to the next over an energy barrier, analogous to the barrier height in the Prandtl-Tomlinson model for sliding friction [12-17]. However, the low value of the sliding potential implies that the KCl film does not have a strong site preference on the Fe(100) substrate suggesting that KCl might not, in fact, be in registry with the Fe substrate and also emphasizes the need for accurate potentials to describe sliding friction.

Although these results show that the previous DFT calculations yield a potential barrier that is in good agreement with the experimentally measured shear strength for KCl films, there are limitations to the predictions that can be made using this approach given the relatively small simulation size and required periodic boundary conditions which force registry. This suggests the use of molecular dynamics (MD) simulations, which have been extensively used to explore the structural and tribological properties of sliding solid-solid interfaces [18-25]. Such simulations have proven extremely useful in helping to understand the behavior of buried interfaces that, in most cases cannot be interrogated directly. However, MD simulations generally use generic potentials that have been optimized to provide reasonable agreement with the experimental results for a wide range of materials, rather than precisely mimicking the behavior of a specific material. When the interfacial structure is controlled by small energy differences, as is the case in the KCl-Fe system, this may result in the prediction of erroneous structures and the resulting properties. Since it is not generally possible to experimentally interrogate the buried sliding

interface, the results of such simulations cannot be directly compared with experiment except to compare predicted parameters such as friction force with the experimental value. It is therefore desirable to tune the interaction parameters in the MD simulation to reproduce experimentally measurable film properties measured for the film-surface interface and then use the tuned simulation to provide information about that interface not available *via* experiment. This is the approach taken in this work. We adjust the interaction potentials between a model alkali halide boundary film on an Fe(100) substrate by comparison with the results of temperature-programmed desorption (TPD) experiments of the desorption behavior of the films. The structure of thin KCl films is then further characterized experimentally using low-energy electron diffraction (LEED) [26] measurements. Finally, the MD simulations, with interaction potentials fitted to the TPD data, are used to explore the influence of contact pressure on the interfacial structure.

2. Methods

1) Experimental Methods

LEED and TPD measurements were carried out in a UHV chamber operating at a base pressure of ~1.3×10^{-8} Pa following bakeout. The chamber was pumped by means of a liquid-nitrogen-trapped diffusion pump, and the chamber contained a double layer of μ-metal, to minimize extraneous magnetic fields inside the vacuum chamber. The Fe(100) single crystal (Princeton Scientific, 99.999 %) purity was initially treated by heating in a hydrogen atmosphere under a pressure of 1 atmosphere at 800 K for ~420 hours to reduce the level of bulk carbon in the sample. The sample was then attached to the end of a co-axial sample manipulator, and could be resistively heated to ~900 K or cooled to ~80 K by contact with a liquid-nitrogen filled reservoir. The sample temperature was measured by means of a chromel/alumel thermocouple spot welded to the edge of the sample. The sample was then cleaned by repeated argon ion bombardment cycles (4μA/cm^2 with a beam energy of 0.5keV) at an elevated sample temperature (600-700 K) followed by annealing (800-900 K). Auger spectroscopy showed that the iron single crystal was clean after this procedure and exhibited a sharp LEED pattern indicating that the surface was well ordered.

Potassium chloride was evaporated from a small (~1 mm internal diameter) alumina tube furnace and the KCl temperature monitored by means of a chromel/alumel thermocouple placed in the KCl pellet to ensure a reproducible evaporation rate, which was monitored by means of a water-cooled, quartz-crystal microbalance in the UHV chamber. The microbalance was mounted to a z-motion drive to allow it to be moved to the same location as the Fe(100) sample to ensure identical KCl fluxes during both source calibration and sample dosing. KCl was deposited with the sample temperature held at ~500 K to provide a uniform KCl film [27].

LEED patterns were collected using a four-grid LEED system (Varian) and recorded with a digital camera. Since KCl is susceptible to electron beam damage where the halide ions are removed *via* a Knotek-Fiebelman [28, 29] mechanism in which a core hole in the halide ion created by the incident electron beam decays to emit an Auger electron, thereby creating an unstable Cl^+ ion, all LEED measurements were made using beam energies that were below the Cl 1s ionization energy.

Temperature-programmed desorption (TPD) data were collected using a heating rate of 5K/s and desorbing species were detected using a (Hiden) quadrupole mass spectrometer whose ionizer was placed in-line-of-sight of the front face of the sample. Both the sample temperature and the ion intensity were collected simultaneously and exported in Excel format. The desorption data were numerically fit to a rate equation of the form $\frac{d\theta}{dt} = -Aexp\left(\frac{E_{act}}{RT}\right)\theta^n$, where A is a pre-exponential factor, E_{act} is the desorption activation energy, Θ is the KCl coverage and n the reaction order, using the experimental heating rate. The rate equation was numerically integrated with temperature steps that were sufficiently small (0.5 K) to yield results that were independent of choice of the temperature step. The parameters were varied to reproduce the experimental desorption maxima and the peak widths and shapes.

2) Molecular Dynamics Simulations

Two computational models were created as shown in Figure 1. Both models contain an Fe substrate with dimensions of 12.0 × 12.0 × 0.6 nm^3. A small slab of an m-layer (m=1, 2,…,14) KCl film with in-plane dimensions of 4.72 × 4.72 nm^2 was placed in the center of the Fe. In Model 1, shown in Figure 1(a), the top surface of the KCl was free. In Model 2, shown in Figure 1(b), a rigid Fe plate, with the same orientation as the bottom Fe surface, was placed on top of the KCl film. During the simulation, the outermost atomic layer of Fe was held fixed. In both models, periodic boundary conditions were applied in the plane parallel to the Fe-KCl interface. Both models were equilibrated by running dynamics for 0.5 ns until the potential energy of the system reached a constant value. Then, the KCl lattice was characterized throughout the film by measuring the distance between two adjacent K (or Cl) atoms in each KCl layer, and by fitting the distribution of the data to a Gaussian function to obtain the mean lattice constant (for the standard unit cell of the NaCl (B1) structure) and its standard deviation. Model 2 was used to investigate the effect of pressure with normal loads of 0.014, 0.14, 1.41 and 14.1 nN applied to the top plate, corresponding to contact pressures of 0.63, 6.30, 63.0 and 630 MPa. The system was equilibrated for 1 ns after each load was applied. We partially validated this model by calculating the Poisson's ratio and elastic modulus from the change in the normal and in-plane dimensions of the innermost four layers of the 8-layer KCl model due to an increase in pressure from 6.3 to 630 MPa. The model predicted a Poisson's ratio of 0.194 and an elastic modulus of 44.8 GPa, which are reasonably consistent with the bulk properties of KCl (Poisson ratio = 0.216; elastic modulus = 38.2 GPa).

The desorption activation energy (E_a) was calculated using Model 1 from the difference in potential energy of the system before and after removing a single KCl pair. E_a was calculated using the equation [30]: $E_a = E_{N\text{-}1,KCl\text{-}Fe} + E_{1,KCl} - E_{N,KCl\text{-}Fe}$, where $E_{N,KCl\text{-}Fe}$ and $E_{N\text{-}1,KCl\text{-}Fe}$ are the potential energies of the system before and after the removal of KCl, respectively, and $E_{1,KCl}$ is the energy of one KCl at equilibrium. The values of $E_{N,KCl\text{-}Fe}$ and $E_{N\text{-}1,KCl\text{-}Fe}$ were calculated directly from the simulation after energy minimization. However, this approach could not be applied to $E_{1,KCl}$ because the empirical potential was fit to crystalline KCl and therefore not expected to be able to predict gas-phase energies, which is the state of the KCl as it is desorbed in the experiment. To address this, we assumed that E_a from MD and experiment should be the same for sufficiently large films, i.e. where the Fe interaction has no effect on activation energy,

and the value of the calculated $E_{1,KCl}$ was adjusted such that the activation energy of the 2.5 nm thick film was the same in the experiment and simulation. We initially tested removing KCl from four different positions on the film, i.e. film center, edge center, and the K- and Cl-terminated corners; see Figure 1(a). The results showed that, for any film thickness, the smallest E_a was always calculated from the model where we removed KCl from one of the two corners. This is consistent with ½ order dependence of the activation energy from the TPD experiment (see below) which suggested atoms were removed from the edge of the KCl slab. Therefore, in subsequent calculations, E_a was identified as the smaller of the values calculated from the two corner positions.

Multiple empirical potentials were used to describe the atomic interactions for the system. The Born-Mayer-Huggins (BMH) [31] potential was used to model interactions within the KCl, with potential parameters from Ref. [32]. The Embedded-Atom Method (EAM) [33, 34] was used to describe Fe, with potential parameters from Ref. [35]. Interactions between KCl and Fe were modeled using the Morse potential: $E = D_0\left[e^{-2\alpha(r-r_0)} - 2e^{-\alpha(r-r_0)}\right]$, where D_0 is the potential well depth, r is the distance between each atom pair, r_0 is the equilibrium distance, and α is the exponential parameter that controls the width of the potential well. The potential parameters were tuned by matching the MD-predicted activation energies with the corresponding experimental results. All simulations were conducted using the open-source software LAMMPS [36].

3. Results and Discussion

1) Activation Energy

a) Temperature-Programmed Desorption Experiments.

A series of temperature-programmed desorption data for KCl evaporated onto Fe(100) at 300 K collected using a heating rate of 5 K/s are displayed in Fig. 2(a) while monitoring 39 amu. The desorption profiles are asymmetric indicating a desorption order of unity or less [37] and show a peak temperature that increases as a function of film thickness from ~639 K for the thinnest films up to ~690 K for a thick KCl layer. The inset to Figure 2(a) shows the integrated peak areas for each of the desorption profiles plotted *versus* the initial film thickness. The linearity of the plot indicates that KCl adsorbs with a constant sticking probability and that a constant flux is provided by the KCl dosing source.

The TPD data were fit by numerically integrating the rate equation:

$$-\frac{d\theta}{dt} = A\theta^n e^{-\frac{E_{act}(\theta)}{k_B T}} \quad (1)$$

where A is a pre-exponential factor, θ the coverage, n the reaction order, $E_{act}(\theta)$ the coverage-dependent desorption activation energy, k_B the Boltzmann constant and T, the temperature. The fit was carried out over small temperature steps using the measured linear heating rate, β = 5K/s to yield:

$$-\frac{d\theta}{dT} = \frac{A}{\beta}\theta^n e^{-\frac{E_{act}(\theta)}{k_B T}} \quad (2).$$

The size of the temperature step was decreased until no changes in the fitting parameters were observed to ensure that the numerical integration of Eqn. (2) was accurate. The values of A, n and $E_{act}(\theta)$ were systematically adjusted to provide the best fit to each desorption profile by minimizing the standard deviation between the theoretical fit and the experimental data. The reaction order n was found to be 0.5 ± 0.1 suggesting that desorption takes place on the perimeters of KCl patches on the surface. The resulting values of the desorption activation energies as a function of film thickness are displayed in Figure 2(b). This initially increases rapidly from a value of ~130 kJ/mol for the thinnest films, rising rapidly with increasing film thickness to reach an almost constant value of ~230 kJ/mol for films thicker than ~0.8 nm, in reasonable agreement with the heat of sublimation of KCl [38].

b) MD and the KCl-Fe Pair Potential.

The experimentally-measured activation energy was used to tune the Morse potential parameters that describe the interactions between KCl and Fe in the MD simulations. We started with thick films, for which the activation energy was unaffected by the iron substrate and therefore determined only by the KCl potential. As shown in Figure 3, the activation energy of the simulation and experiment are necessarily the same for the thickest films (~2.5 nm). As the film thickness decreased, the activation energy decreased and the rate of this decrease was determined in the simulation by the KCl-Fe potential. The initial Morse parameters (D_0, α and r_0) were obtained by reproducing the change of energy with distance between KCl and Fe slabs from the previous DFT calculations [11, 39, 40]. We then tuned the minimum energy for the K-Fe and Cl-Fe interactions ($D_{0,K\text{-}Fe}$ and $D_{0,Cl\text{-}Fe}$) to match the experimentally measured activation energy for films between 0.3 and 1.2 nm thick. The other two parameters (α and r_0) were unchanged from their initial values ($\alpha_{K\text{-}Fe}$ =9.8 nm^{-1}, $r_{0,K\text{-}Fe}$ = 0.421 nm, $\alpha_{Cl\text{-}Fe}$ = 14.0 nm^{-1} and $r_{0,Cl\text{-}Fe}$ = 0.270 nm). We observed that activation energy increased monotonically with increasing KCl-Fe interaction strength and that the rate of that increase was faster for thinner films and for stronger interactions. The best fit values of the minimum energy parameter were found to be: $D_{0,K\text{-}Fe}$ = 0.67 kJ/mol and $D_{0,Cl\text{-}Fe}$ = 8.74 kJ/mol. Note that we did not model films with thicknesses smaller than the lattice constant of a single layer since those corresponded to experimental measurements of partial films which could not be reproduced reliably in the simulations. Figure 3 shows that the activation energy predicted from MD using the best fit Morse parameters for films at least one layer thick was in good agreement with the values obtained from TPD.

2) Film Structure

a) LEED Patterns.

Low-energy electron diffraction images were obtained for thin KCl films to avoid sample charging, which was further minimized by keeping the beam current as low as possible. Figure 4(a) shows the LEED pattern for clean Fe(100) collected using a beam energy of ~50 eV. This displays a square pattern expected of the Fe(100) face and is used to calibrate the spacing of KCl films using the standard lattice constant for Fe of 0.287 nm [41].

Figure 4(b) shows the corresponding LEED pattern for 1 monolayer (ML) of KCl deposited onto iron at ~500 K, also collected using the same beam energy of 50 eV, showing both the Fe(100) substrate spots and those due to KCl. Here the substrate spots are circled in red and yield the same spot spacing as in Figure 2(a) confirming that identical electron beam energies were used in both cases. The additional spots due to KCl are aligned with the Fe(100) substrate. Comparing the spot spacings with those of the underlying Fe(100) substrate gives the lattice constant for the KCl monolayer to yield a K–K (or Cl–Cl) distance of 0.48 ± 0.01 nm (compared with 0.4449 nm for pure KCl) [41]. This suggests that the first layer KCl is slightly expanded compared to the bulk KCl lattice.

Figure 4(c-e) display the LEED pattern from two, three and four monolayers of KCl on Fe(100), again collected using a beam energy of 50 eV, where now the Fe(100) substrate diffraction spots are obscured. The LEED patterns are slightly distorted since the electron beam is not normal to the surface. However, the spacings between the diffraction spots are identical for all three films indicating that a bulk-like KCl film is formed when the film thickness is greater than or equal to two monolayers. In addition, the measured spot spacings are consistent with the bulk lattice structure of KCl. This implies that the interaction potential between the KCl film and the underlying Fe(100) lattice is small since a two-layer film of KCl provides sufficient elastic energy to overcome the small lattice distortion (of ~7 %) found for the first monolayer. Note that even the distorted first-monolayer film is not in registry with the substrate.

b) MD Modeled KCl with a Free Surface

In the simulations, Model 1 was used to study the equilibrium structure of KCl films between 1 and 14 layers thick. Because of the atomic-level detail available in the simulation, we were able to observe the variation of this structure, both between and within the KCl layers in a given film. Therefore, we characterized the distribution of in-plane lattice constants for each film, using a Gaussian fit to estimate mean values and their standard deviations. Figure 5(a) shows a representative distribution and fit for eight-layer KCl. In this case, the mean lattice constant is comparable to the value predicted for the bulk material using the BMH potential (0.625 nm) and the standard deviation is small, indicating that most of the film conforms to the bulk material structure. The mean of the lattice constant for films between 1 and 14 layers thick is shown in Figure 5(b). The mean lattice constants of the thicker model films are comparable to that of bulk KCl, consistent with the LEED pattern for KCl films of two monolayers and thicker. Note that the mean values reported here were calculated from Gaussian fits to atom positions throughout the film, including the edges of the film where variation from bulk structure is expected. However, recalculation using only the middle 75% of the films yielded slightly smaller error bars, but similar mean values and the same trends.

However, as the film thickness decreases, so too does the mean lattice constant of the film. For the two-layer film, the mean lattice constant is 0.611nm, which is between that of bulk KCl and bulk Fe. This result differs from the LEED pattern which indicated the two-layer film exhibited the bulk KCl lattice. The mean lattice constant of the model film reflects the relatively large variation of the structure within and between the two layers of KCl. This is reflected by the large error bar for this case in Figure 5(b). It can also be observed from the distribution of the lattice

constants in each layer of the model film, which is shown as a contour plot in Figure 6 for a smaller KCl patch (2.2 nm × 2.2 nm) to highlight key trends. The contour plot for each given layer was generated by calculating the in-plane mid-point position and the in-plane distance between each pair of adjacent K (or Cl) atoms. The color on the plots represents the magnitude of the distance (lattice) at each mid-point position, with color between calculated values obtained using interpolation.

Figure 6 shows that the first KCl layer (adjacent to the Fe) is predominantly in registry with the Fe, particularly near the center of the film, while the second layer largely reflects the KCl lattice. It is noted that the escape depth for 50-eV electrons used for the LEED measurements is ~0.4 nm and thus predominantly probes just the outermost layer of the KCl film. The difference between the structure of thin films in the experiment and simulation is even more obvious in the single-layer film. In the simulations, the single layer KCl mean lattice constant was found to be 0.572 nm, i.e. similar to bulk Fe, indicating that the KCl is in registry with the Fe substrate. This contrasts with the LEED results which suggest that the single layer KCl lattice is larger than that of both bulk Fe and KCl. We were unable to reproduce this observation with any values of the Morse parameters: with strong interactions, the KCl was in registry with the Fe as expected for the Morse pair potential; but with weak interactions, the BMH potential that was fitted to bulk KCl was unable to maintain the single layer structure resulting in a buckling of the film. This issue might be addressed by using a non-pairwise, or location dependent KCl-Fe potential, but is out of the scope of this study.

c) Effect of Pressure on Interfacial Structure

Next we used the simulations to explore the effect of pressure on the structure of KCl confined between two Fe surfaces (Model 2). We analyzed only films with four layers or more since, as shown in the previous section, thinner model films exhibited structures that differed from the LEED measurements. First we analyzed the variation of structure across the film. The mean in-plane lattice in each layer of an eight-layer KCl slab as a function of load is shown in Figure 7. At any load, the smallest lattice is observed in layers adjacent to the Fe and the largest in the middle of the film. Comparing the structure of the film at the two loads, we observe that the mean lattice constant of the outermost layers decreases with load while that of the innermost layers increase with load. This suggests that, as load increases, the outermost KCl layers are forced into registry with the Fe, and that the inner KCl layers respond to this strain by expanding. The net effect is that there is a slight increase in the overall lattice of the film as the load increases (see dashed lines in Figure 7).

These trends are illustrated in another way in Figure 8, which plots the effect of load on the in-plane lattice averaged over the entire eight-layer film, and only the innermost two layers or only the outermost two layers; the mean lattice constant of the free surface film is also shown for reference. Consistent with the trends shown in Figure 7, we observe that the overall mean lattice constant of the confined film is larger than that of the free surface film at any load, and increases slightly with increasing load. This trend is attributable to combined effects of the load-induced increase in the lattice constant of the inner layers and decrease of the lattice constant in the outer layers.

The trends observed for the eight-layer case are also exhibited by the other films. The percent change in the in-plane lattice due to confinement and due to an increase in load by a factor of 1000 for films up to fourteen layers thick is shown in Figure 9. The hollow symbols represent the change in the lattice of just the outermost layers, which is negative (smaller lattice) for all films and is relatively constant with varying film thickness. The effect of confinement and load on the overall mean lattice, however, is affected by film thickness. Except for the four-layer film, the change in mean lattice is positive (larger lattice) due to both confinement and load, and these effects increase with film thickness, approaching a constant value above approximately ten layers. Although all of these changes are very small (<1%), since the thicker films have more inner layers, the trends are consistent with the suggestion that load is partially accommodated by expansion of the inner layers of a confined film.

4. Conclusions

A simple model system consisting of KCl films on a clean iron surface was used to investigate the effects of thickness and pressure on film structure. The study was performed with both experiments and molecular dynamics simulations. The simulations used existing empirical potentials to describe the KCl film and Fe substrate, but the critical interactions between the film and substrate were tuned to match the corresponding experimental system. This was accomplished by performing TPD measurements and fitting that data to a rate equation to yield film thickness-dependent desorption activation energy. The desorption activation energy was then predicted by the simulations, and the minimum energy in the pair potential that was used to describe the KCl-Fe interactions was tuned such that the model predictions were consistent with the data obtained from experiment.

LEED measurements KCl films indicated that two-layer films and thicker films exhibited the structure of bulk KCl while the single layer film adopted a structure distorted by the adjacent Fe. A model structure of the single layer KCl film was proposed based on the LEED observations. Unfortunately, simulations were unable to reproduce the structure indicated by the experiments of the thinnest films, instead predicting the first layer of the film would be in registry with the Fe. This is likely a limitation of the pair potential used to model the KCl-Fe interaction. However, simulations of thicker films did predict a mean lattice constant consistent with the bulk materials, consistent with the two-layer LEED measurements (and similar results assumed for thicker films).

Simulations of films at least four layers thick were then used to investigate the effect of pressure on film and interface structure. Pressure was found to decrease the lattice constant of the outermost layers of the film while increasing the lattice constant of the film's inner layers. These trends were observed for all films, where the effect of pressure on the inner layer was more significant for thicker films. These results suggest an additional possible origin for the pressure-dependence of shear strength. It was previously suggested that the vertical motion associated with sliding from one potential minimum to the next on the surface resulted in additional external work being carried out on the system, thereby yielding a pressure-dependent shear strength. However, the above simulations, combined with the experimental results for the film-

vacuum interface, suggest an additional possibility, that of a change in interfacial registry at higher contact pressures. Since the shear strength has been found to increase when the boundary film and the substrate are in registry, the increasing registry between the film and substrate at higher pressure can also be expected to result in an increase in shear strength with pressure. Clearly, both effects can occur simultaneously and MD simulations of sliding are currently being carried out to explore these effects as well as the influence of interfacial dynamics on the registry between the film and substrate.

Acknowledgements. We gratefully acknowledge support by the National Science Foundation under grant number CMMI-1265742

References

[1] M. Hirano, K. Shinjo, Atomistic locking and friction, Physical Review B, 41 (1990) 11837-11851.
[2] M.H. Muser, L. Wenning, M.O. Robbins, Simple microscopic theory of Amontons's laws for static friction, Physical Review Letters, 86 (2001) 1295-1298.
[3] M.H. Muser, Structural lubricity: Role of dimension and symmetry, Europhys. Lett., 66 (2004) 97-103.
[4] M.H. Müser, M.O. Robbins, Conditions for static friction between flat crystalline surfaces, Physical Review B, 61 (2000) 2335-2342.
[5] M. Peyrard, S. Aubry, Critical behaviour at the transition by breaking of analyticity in the discrete Frenkel-Kontorova model, Journal of Physics C: Solid State Physics, 16 (1983) 1593.
[6] T. Filleter, W. Paul, R. Bennewitz, Atomic structure and friction of ultrathin films of KBr on Cu(100), Physical Review B, 77 (2008) 035430.
[7] F. Gao, O. Furlong, P.V. Kotvis, W.T. Tysoe, Pressure dependence of shear strengths of thin films on metal surfaces measured in ultrahigh vacuum, Tribol. Lett., 31 (2008) 99-106.
[8] B.J. Briscoe, D.C.B. Evans, The Shear Properties of Langmuir-Blodgett Layers, Proceedings of the Royal Society of London. A. Mathematical and Physical Sciences, 380 (1982) 389-407.
[9] A. Erdemir, R.A. Erck, J. Robles, Relationship of hertzian contact pressure to friction behavior of self-lubricating boric acid films, Surface and Coatings Technology, 49 (1991) 435-438.
[10] M.H. Müser, Lubricants under high local pressure: Liquids act like solids, Materialwissenschaft und Werkstofftechnik, 35 (2004) 603-609.
[11] M. Garvey, O.J. Furlong, M. Weinert, W.T. Tysoe, Shear properties of potassium chloride films on iron obtained using density functional theory, J. Phys.-Condes. Matter, 23 (2011) 265003.
[12] L. Prandtl, Ein Gedankenmodell zur kinetischen Theorie der festen Körper., Z. Angew. Math. Mech., 8 (1928) 85.
[13] G.A. Tomlinson, A Molecular Theory of Friction, Phil. Mag., 7 (1929) 905.
[14] E. Gnecco, R. Bennewitz, A. Socoliuc, E. Meyer, Friction and wear on the atomic scale, Wear, 254 (2003) 859-862.
[15] C. Fusco, A. Fasolino, Velocity dependence of atomic-scale friction: A comparative study of the one- and two-dimensional Tomlinson model, Physical Review B, 71 (2005) 045413.

[16] O.J. Furlong, S.J. Manzi, V.D. Pereyra, V. Bustos, W.T. Tysoe, Monte Carlo Simulations for Tomlinson Sliding Models for Non-Sinusoidal Periodic Potentials, Tribol. Lett., 39 (2010) 177-180.
[17] M. Müser, Velocity dependence of kinetic friction in the Prandtl-Tomlinson model, Physical Review B, 84 (2011) 125419.
[18] J.A. Harrison, D.W. Brenner, Simulated Tribochemistry - An Atomic Scale View of the Wear of Diamond, Journal of the American Chemical Society, 116 (1994) 10399-10402.
[19] G.T. Gao, P.T. Mikulski, J.A. Harrison, Molecular-scale tribology of amorphous carbon coatings: Effects of film thickness, adhesion, and long-range interactions, Journal of the American Chemical Society, 124 (2002) 7202-7209.
[20] W.B. Donald, A.S. Olga, A.H. Judith, J.S. Steven, N. Boris, B.S. Susan, A second-generation reactive empirical bond order (REBO) potential energy expression for hydrocarbons, Journal of Physics: Condensed Matter, 14 (2002) 783.
[21] J.A. Harrison, G. Gao, J.D. Schall, M.T. Knippenberg, P.T. Mikulski, Friction between solids, Philosophical Transactions of the Royal Society A: Mathematical, Physical and Engineering Sciences, 366 (2008) 1469-1495.
[22] Y. Dong, Q. Li, J. Wu, A. Martini, Friction, slip and structural inhomogeneity of the buried interface, Model. Simul. Mater. Sci. Eng., 19 (2011).
[23] Y. Dong, Q. Li, A. Martini, Molecular dynamics simulation of atomic friction: A review and guide, Journal of Vacuum Science & Technology A, 31 (2013) 030801.
[24] S.B. Sinnott, S.-J. Heo, D.W. Brenner, J.A. Harrison, Computer Simulations of Nanometer-Scale Indentation and Friction, Nanotribology and Nanomechanics, Springer Berlin Heidelberg2008, pp. 655-740.
[25] I. Szlufarska, M. Chandross, R.W. Carpick, Recent advances in single-asperity nanotribology, Journal of Physics D: Applied Physics, 41 (2008) 123001.
[26] M.A. Van Hove, S.Y. Tong, Surface crystallography by LEED : theory, computation, and structural results, Springer-Verlag, Berlin; New York, 1979.
[27] F. Gao, G. Wu, D. Stacchiola, M. Kaltchev, P.V. Kotvis, W.T. Tysoe, The tribological properties of monolayer KCl films on iron in ultrahigh vacuum: Modeling the extreme-pressure lubricating interface, Tribol. Lett., 14 (2003) 99-104.
[28] M.L. Knotek, P.J. Feibelman, Ion Desorption by Core-Hole Auger Decay, Physical Review Letters, 40 (1978) 964-967.
[29] P.J. Feibelman, M.L. Knotek, Reinterpretation of electron-stimulated desorption data from chemisorption systems, Physical Review B, 18 (1978) 6531-6539.
[30] H. Zhang, J.R. Rustad, J.F. Banfield, Interaction between Water Molecules and Zinc Sulfide Nanoparticles Studied by Temperature-Programmed Desorption and Molecular Dynamics Simulations, The Journal of Physical Chemistry A, 111 (2007) 5008-5014.
[31] M.J.L. Sangster, M. Dixon, Interionic potentials in alkali halides and their use in simulations of the molten salts, Advances in Physics, 25 (1976) 247-342.
[32] M.C.C. Ribeiro, Chemla Effect in Molten LiCl/KCl and LiF/KF Mixtures, The Journal of Physical Chemistry B, 107 (2003) 4392-4402.
[33] M.S. Daw, M.I. Baskes, Embedded-atom method: Derivation and application to impurities, surfaces, and other defects in metals, Physical Review B, 29 (1984) 6443-6453.
[34] M.S. Daw, M.I. Baskes, Semiempirical, Quantum Mechanical Calculation of Hydrogen Embrittlement in Metals, Physical Review Letters, 50 (1983) 1285-1288.

[35] M.I. Mendelev, S. Han, D.J. Srolovitz, G.J. Ackland, D.Y. Sun, M. Asta, Development of new interatomic potentials appropriate for crystalline and liquid iron, Philosophical Magazine, 83 (2003) 3977-3994.
[36] S. Plimpton, Fast Parallel Algorithms for Short-Range Molecular Dynamics, Journal of Computational Physics, 117 (1995) 1-19.
[37] P.A. Redhead, Thermal desorption of gases, Vacuum, 12 (1962) 203-211.
[38] M.W. Chase, S. National Institute of, Technology, NIST-JANAF thermochemical tables, American Chemical Society ; American Institute of Physics for the National Institute of Standards and Technology, [Washington, D.C.]; Woodbury, N.Y., 1998.
[39] M. Garvey, M. Weinert, W.T. Tysoe, On the Pressure Dependence of Shear Strengths in Sliding, Boundary-Layer Friction, Tribol. Lett., 44 (2011) 67-73.
[40] M. Garvey, M. Weinert, W.T. Tysoe, On the film thickness dependence of shear strengths in sliding, boundary-layer friction, Wear, 274–275 (2012) 281-285.
[41] R.W.G. Wyckoff, Crystal structures, Interscience Publishers, New York, 1963.

Figure Captions

Figure 1: Snapshots of the two MD models. (a) In Model 1, the top surface of the KCl is free. White dashed circles identify representative positions (i.e. film center, edge center, K- and Cl-terminated corners) from which KCl was removed to calculate activation energy. (b) The KCl film is confined between two Fe plates in Model 2 with varying normal loads applied to the upper plate.

Figure 2: (a): Temperature-programmed desorption (TPD) data collected by monitoring 39 am for KCl adsorbed on a Fe(100) surface at 300 K collected using a heating rate of 5 K/s and a function of KCl films thickness. The inset shows a plot of the integrated peak area as a function of film thickness. (b) Plot of desorption activation energy as a function of films thickness obtained by fitting the desorption profiles shown in Figure 2(a).

Figure 3: MD-predicted and experimentally-measured activation energies as functions of film thickness.

Figure 4: LEED patterns collected using a beam energy of 50 eV for (a): a clean Fe(100) surface, (b) 1 ML of KCl on Fe(100). The spots due to the Fe(100) substrate are circled in red, while the additional features are due to KCl. (c) 2 ML of KCl of Fe(100) (d) 3 ML of KCl on Fe(100) and (e) 4 ML of KCl on Fe(100). The substrate spots are no longer visible in the last three diffraction patterns and the spots are due only to the KCl film.

Figure 5: a) Distribution of in-plane lattice constants within an eight-layer KCl film, fit to a Gaussian function to enable calculation of the mean and standard deviation. (b) Mean in-plane lattice constant for KCl films of varying thickness.

Figure 6: Contour plots of the in-plane lattice in each of the two layers of two-layer KCl illustrating the variation of the structure of the film, both within and between the layers.

Figure 7: Structure of the eight-layer confined KCl film at two different normal loads. Points represent the mean in-plane lattice constant in each layer of the film where layers 1 and 8 are adjacent to the Fe, and dashed lines represent the overall mean in-plane lattice of the confined film subject to load and with one free surface.

Figure 8: Variation of the mean in-plane lattice constant of the KCl films due to load. The mean in-plane lattice constant is reported for the entire film and for the innermost and outermost layers of that film. The free surface film in-plane lattice constant is shown for reference.

Figure 9: Change in the mean in-plane lattice constant of a film (solid symbols) and outermost layers (hollow symbols) of that film due to confinement (blue triangles) and a 100 fold increase in load (red circles).

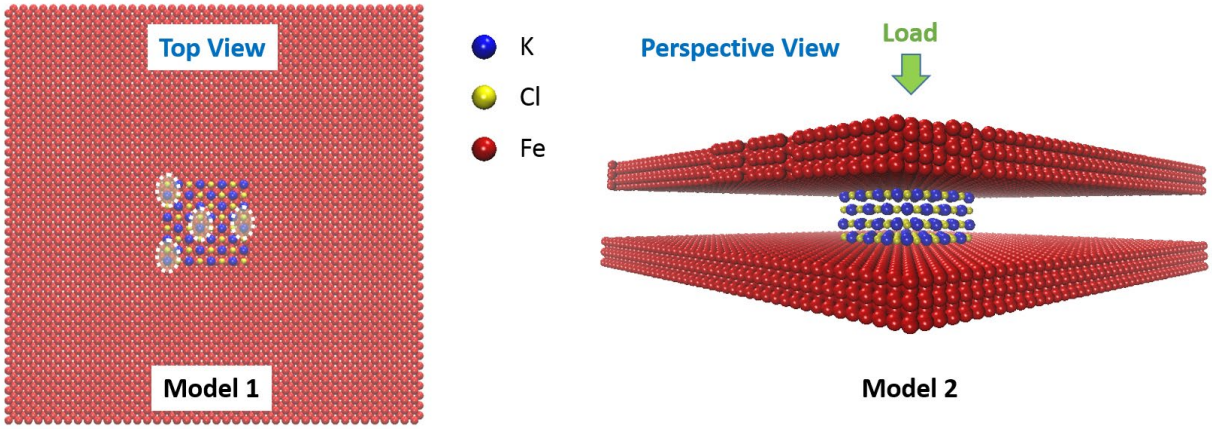

(a) (b)

Olson *et al*, Figure 1.

(a)

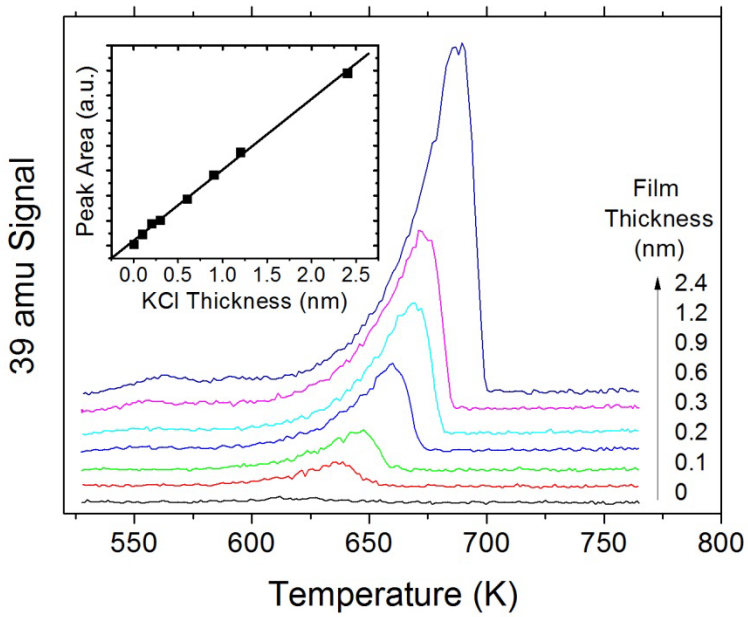

(b)

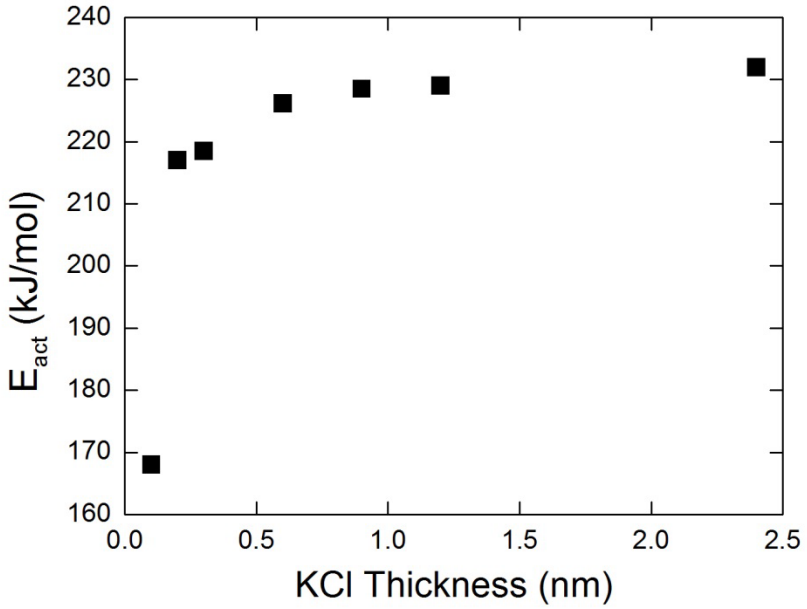

Olson *et al*, Figure 2.

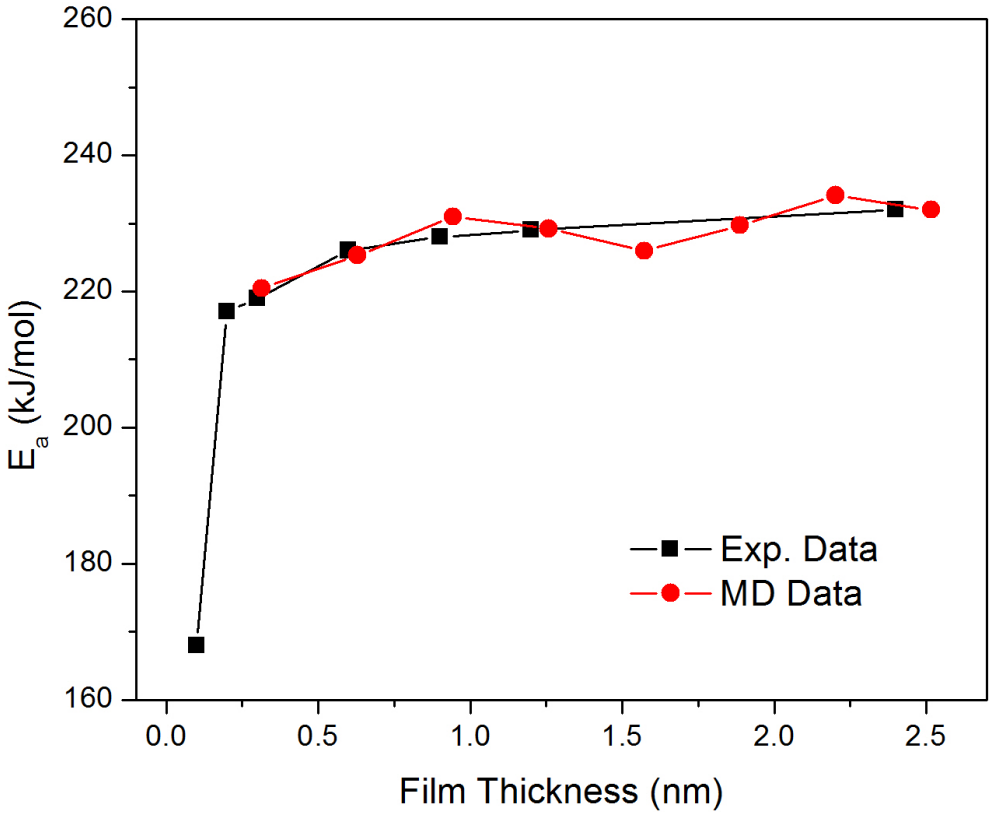

Olson *et al*, Figure 3.

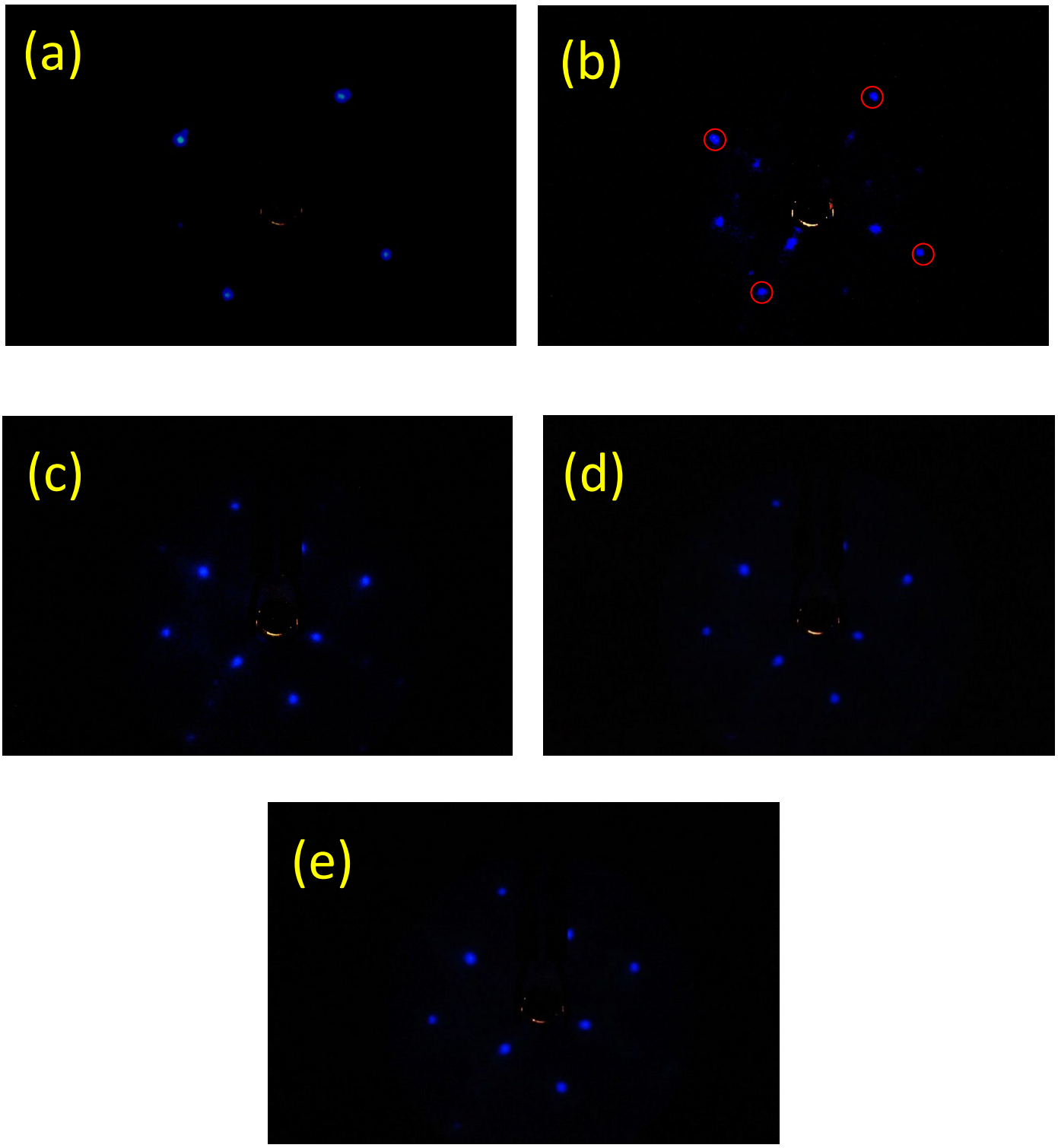

Olson *et al*, Figure 4.

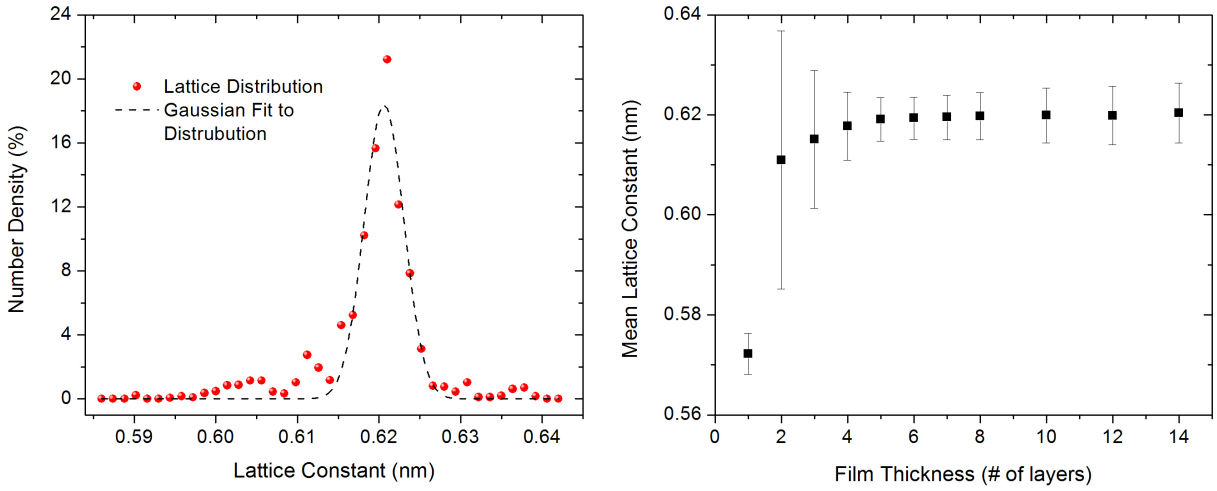

(a) (b)

Olson *et al*, Figure 5.

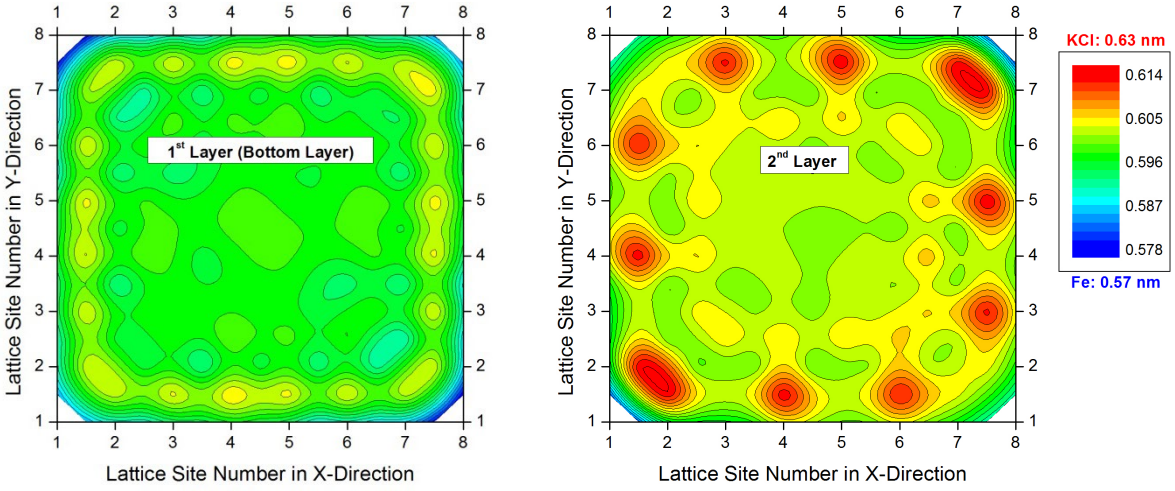

(a) (b)

Olson *et al*, Figure 6.

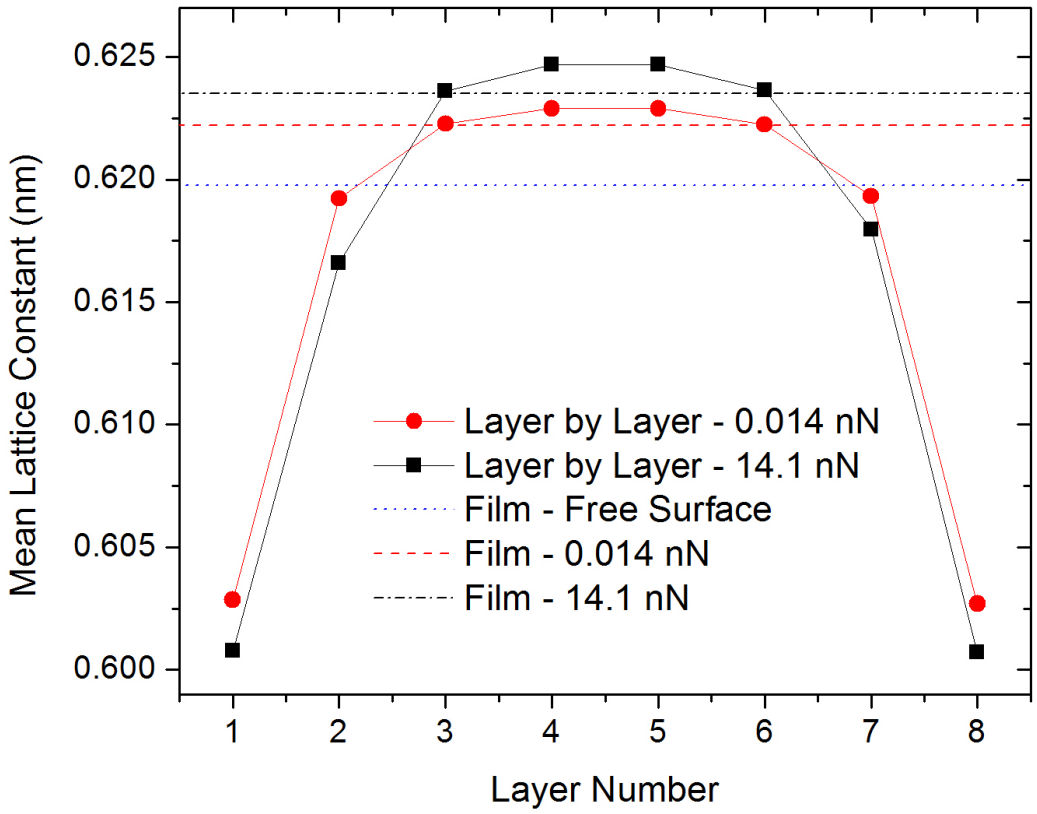

Olson *et al*, Figure 7.

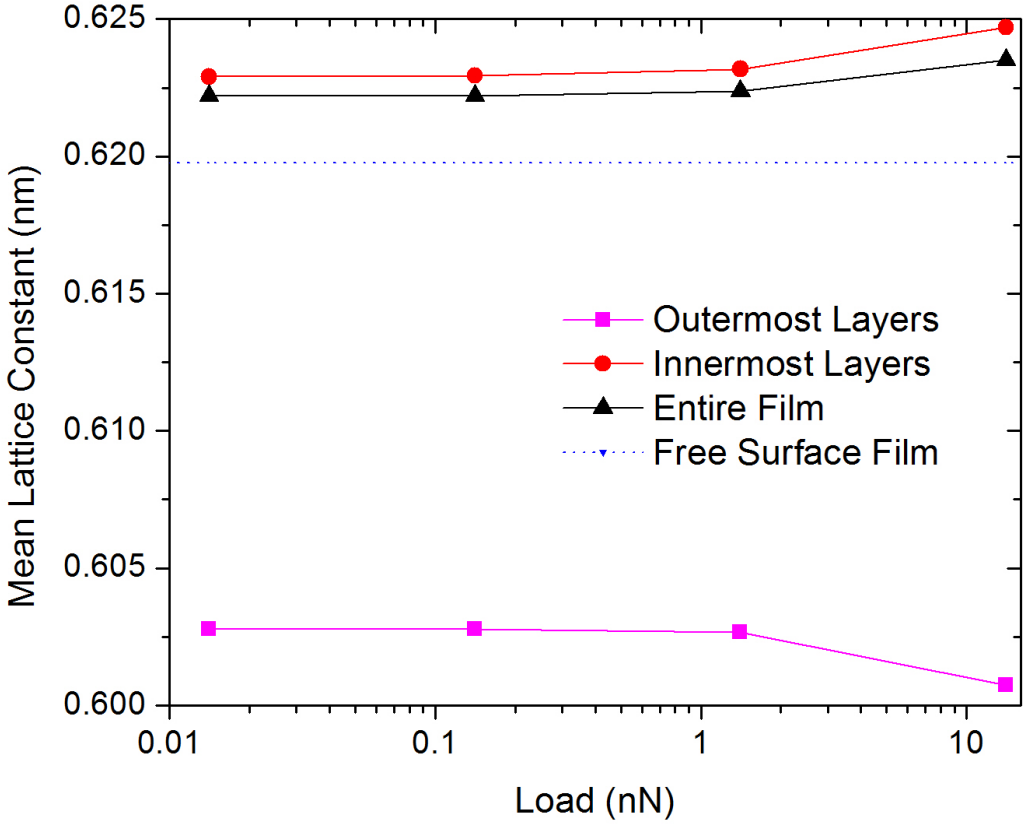

Olson *et al*, Figure 8.

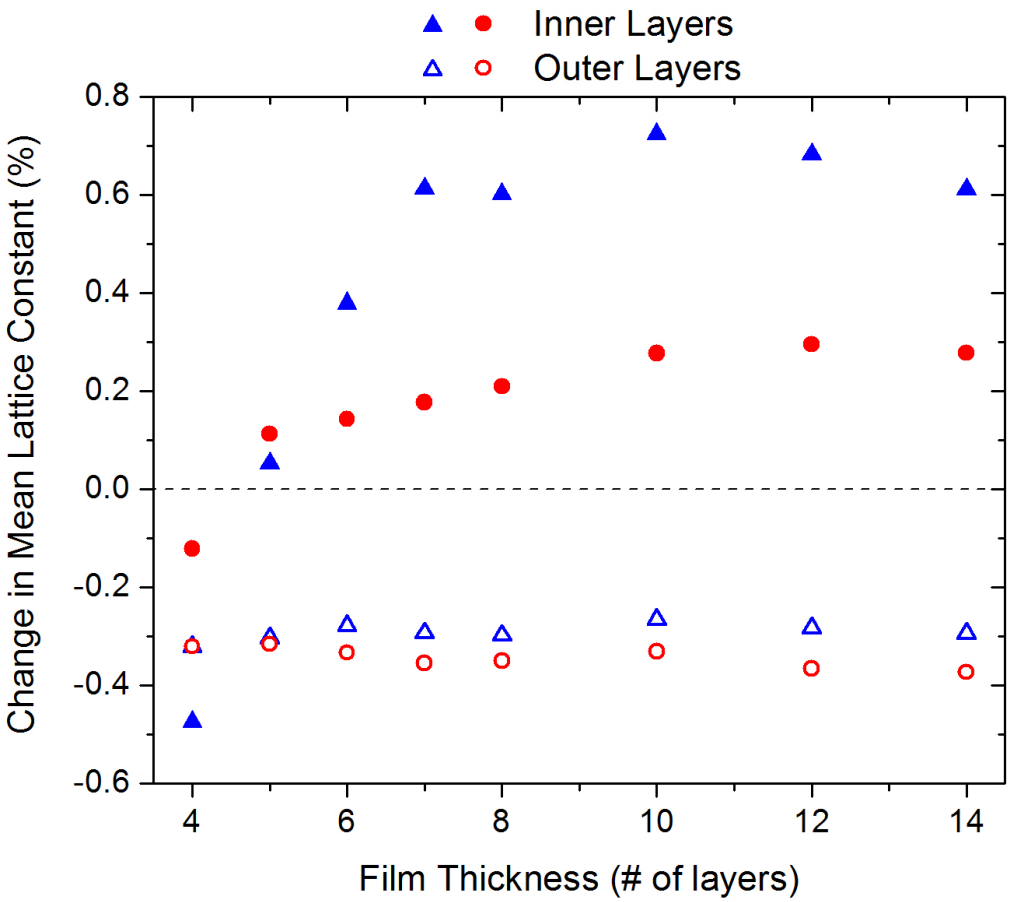

Olson *et al*, Figure 9.